

# Enlarged bilayer interfaces from liquid-liquid dewetting for photovoltaic applications

Jakob Heier<sup>\*a</sup>, Jan Groenewold<sup>b</sup>, Fernando A. Castro<sup>a</sup>, Frank Nüesch<sup>a</sup>, Roland Hany<sup>\*a</sup>

<sup>a</sup>Empa, Swiss Federal Laboratories for Materials Test and Research, Laboratory for Functional Polymers, Ueberlandstr. 129, CH-8600 Duebendorf, Switzerland; <sup>b</sup>Physical & Colloid Chemistry, University of Utrecht, Padualaan 8, 3584CH Utrecht, The Netherlands

## ABSTRACT

The details of the arrangement of mixtures of semiconducting materials in thin-films have a major influence on the performance of organic heterojunction solar cells. Here, we exploit the phenomenon of spinodal dewetting during spin coating of blends of PCBM and a cyanine dye for the design of phase separated morphologies with increased interfacial area. AFM snapshots of as-prepared films and after selective dissolution suggest that the solution separates into transient bilayers, which destabilize due to long-range intermolecular interactions. We propose that film destabilization is effectively driven by electrostatic forces that build up due to mobile ions that cross the junction and dissolve partially in PCBM. The resulting morphology type is mainly dependent on the ratio between the layer thicknesses, whereas the dominant wavelengths formed are determined by the absolute film thickness. Solar cells were fabricated from films with known structure and a power conversion efficiency of  $\eta = 0.29\%$  was measured for a vertically segregated film consisting of a cyanine layer covering the anode and an upper phase composed of dewetted PCBM domains. We explain the merits of this structure in contrast to a lateral separated blend morphology where the efficiency was 3 times smaller.

**Keywords:** liquid-liquid dewetting, PCBM, cyanine dye, organic photovoltaic, organic solar cell

## INTRODUCTION

Thin films of blends of organic materials are often used in optoelectronic device applications. Thereby, readily available components with complementary properties can be mixed, and the difficulty of integrating all necessary functionalities in one single material is bypassed. For example, a mixture of a semiconducting electron donor and electron acceptor is widely used as the active layer in all-organic solar cells<sup>1,2</sup>. For high solar energy conversion, the materials need i) to absorb a large part of the solar photons, ii) to have carefully balanced redox levels that allow for charge generation at the molecular heterojunctions, and iii) to transport the charges efficiently to the collecting electrodes.

The morphology and phase separation on the nanometer level between the two components critically determines the charge generation and transport yield. To optimize electron and hole transfer within the  $\sim 10$  nm diffusion range of the primary photoexcitation, a fine-scale blending is desirable; on the other hand, efficient charge transport requires a percolating bicontinuous network with selective contacts to the electrodes. Therefore, efforts aim at fabricating bilayer structures with high aspect ratio interdigitated interfaces in a controlled way<sup>3,4</sup>.

We recently employed surface-directed spinodal demixing of a polymer mixture to create bilayer interface undulations at small length scales for organic photovoltaic applications<sup>5,6</sup>. We identified the mechanisms that lead to submicron interface structures during spin coating of a polymer blend. Bulk spinodal decomposition was the structure-determining process for large polymer molecular weights and lead to a rather coarse interface structure. Only when surface

[roland.hany@empa.ch](mailto:roland.hany@empa.ch), phone +41 44 8234084, fax +41 44 8234012; [jakob.heier@empa.ch](mailto:jakob.heier@empa.ch), phone +41 44 8234356, fax +41 44 8234012

segregation favoured macroscopic phase separation into a bilayer, submicron interfacial structures could be observed. The rough heterojunction interface turned out to be beneficial, and photovoltaic efficiencies increased by a factor of 3 compared to the smooth layer-by-layer configuration.

Here, we explore the possibility to create submicron phase separated structures via dewetting of thin molecular blend films<sup>7-10</sup>. For systems that initially separate into bilayers, effective molecular interactions between surfaces and interfaces can play a distinct role upon solvent evaporation and destabilize the thinning film. The instability can occur at the top surface, the bilayer interface, or at both layers simultaneously. Which of the instabilities is amplified is in a complex way dependent on the film thicknesses, the substrate properties, the volatility of the solvent and the interactions between the material components and their compatibility with the solvent. If the dispersive force driving the instability is not counterbalanced by the inherent energy cost of having a large interface, the films break up and liquid-liquid dewetting patterns with a characteristic spinodal wavelength are observed.

We used a molecular cyanine dye/ $C_{60}$ -derivative (PCBM) blend system for the preparation of photoactive films. Cyanines are a class of charged polymethine dyes processable from solution, which display high extinction coefficients and tunable absorption from the visible to the near-infrared region through structural modification<sup>11</sup>. PCBM is a soluble fullerene derivative and is, for example, widely used as the electron accepting component in high-performing polythiophene blend solar cells<sup>12</sup>. During spin coating, the cyanine/PCBM solution phase separates into a bilayer, and upon solvent evaporation, the film thins and the interface destabilizes. The final morphology consists of phase separated domains of PCBM and cyanine, which were imaged with AFM. We show examples for the variation of morphologies as a function of blend composition, and propose that electrostatic forces at the liquid-liquid interface are the origin of the film destabilization. Finally, we fabricated solar cells using these prototype cyanine/PCBM thin films and correlated the device performance with the degree of phase separation and type of morphology.

## EXPERIMENTAL

PCBM (> 99 %) was purchased from Solenne, and the cyanine dye 1,1'-diethyl-3,3',3'-tetramethylcarbocyanine perchlorate (CyC) was synthesized in our laboratory (Fig. 1). Films were prepared by spin coating blends in chlorobenzene or chloroform on glass or on PEDOT-coated ITO/glass for the fabrication of solar cells. Thicknesses were varied by adjusting the concentrations and spinning conditions. AFM measurements were performed on a Nanosurf

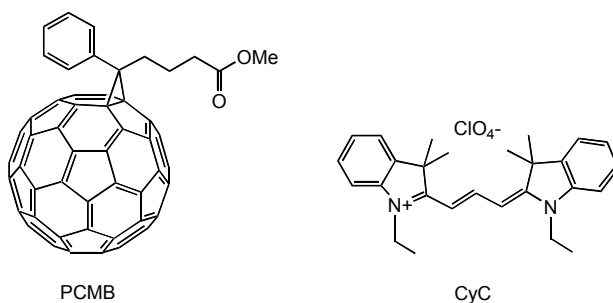


Fig.1. Molecular structure of the soluble fullerene derivate PCBM ([6,6]-phenyl  $C_{60}$ -butyric acid methyl ester) and the cyanine dye CyC with the free counter ion  $ClO_4^-$ .

Mobile S instrument in tapping mode at a resonance frequency of 170 kHz using rectangular silicon cantilevers with a tip radius of curvature of  $\sim 10$  nm. Samples were analysed using WsXM scanning probe microscopy software<sup>13</sup>. Samples were immersed in hexane or 2,2,3,3-tetrafluoropropanol to selectively remove PCBM or CyC from the film. Average film thicknesses were determined with UV-VIS spectroscopy (measured on a Varian Cary 50 spectrophotometer); a

known film area was dissolved in chlorobenzene, and the absorption spectrum was fitted to the spectra of solutions of the individual components, which were obtained from pure films with known thicknesses from AFM. Surface energies of the solid films were obtained from the advancing contact angles of droplets of different liquids (water, cis-decalin, n-hexane, glycerol) after the method of Owens, Wendt, Rabel and Kaelble<sup>14,15</sup>. X-ray photoelectron spectroscopy was performed on a PHI-Quantum 2000 “imaging XPS” to prove that the  $\text{ClO}_4^-$  ions percolate the PCMB material. Photovoltaic devices were fabricated in an ITO/PEDOT/CyC:PCBM/ $\text{C}_{60}$ /Al sandwich structure. The device fabrication procedure and characterization unit is described in Ref. 5.

The individual Hamaker constants were obtained from the experimentally determined surface tensions  $\gamma_i$  as  $A_{ii} = 24\pi\gamma_i D^2$ , where  $D$  is the cutoff intermolecular separation  $D = 0.165 \text{ nm}^{16}$ . With the indices  $s$  referring to substrate (glass),  $1$  = cyanine layer,  $2$  = PCBM layer,  $g$  = gas (air), we calculated  $A_s = 1.3 \cdot 10^{-19} \text{ J}$  ( $\gamma_s = 64.46 \text{ mN m}^{-1}$ ),  $A_1 = 7.0 \cdot 10^{-20} \text{ J}$  ( $\gamma_1 = 34.30 \text{ mN m}^{-1}$ ),  $A_2 = 4.9 \cdot 10^{-20} \text{ J}$  ( $\gamma_2 = 23.9 \text{ mN m}^{-1}$ ), and  $A_g$  is 0. From there the effective Hamaker constants for the bilayer film system,  $A_{g21s}$ ,  $A_{21s}$  and  $A_{12g}$ , were approximated with the individual constants as  $A_{ijkl} = (\sqrt{A_{ii}} - \sqrt{A_{kk}}) \times (\sqrt{A_{ii}} - \sqrt{A_{jj}})$  and  $A_{ijk} = (\sqrt{A_{ii}} - \sqrt{A_{jj}}) \times (\sqrt{A_{kk}} - \sqrt{A_{jj}})$ .

## RESULTS

Fig. 2 shows typical dewetting patterns of thin PCBM/CyC films. The blends phase separate during spin coating and domains of one component are embedded in the matrix of the other material. With the solvents hexane or 2,2,3,3-tetrafluoropropanol either PCBM (Fig. 2B,F) or CyC (data not shown) could be selectively dissolved, and, with these

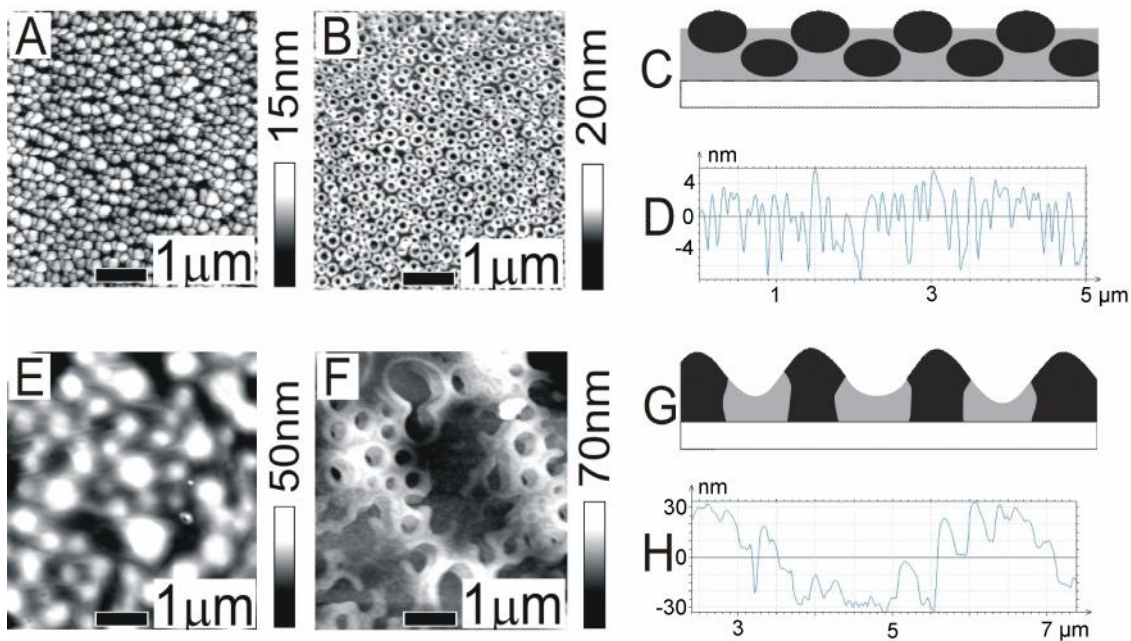


Fig. 2. AFM scans of PCBM/CyC films spin coated from chlorobenzene solution on glass. A) as-prepared film with an average thickness of 36 nm for PCBM and 56 nm for CyC; B) same film after removal of PCBM by immersion for 3 minutes in hexane; C) schematic diagram of the dewetting pattern; D) typical AFM cross section of the remaining CyC layer shown in Fig. 2B. E) – H) same sequence as above for a film with an average thickness of 55 nm both for PCBM and CyC. Qualitatively, the same patterns were observed for films spin coated on PEDOT-coated ITO/glass.

complementary data, a morphology picture can be constructed. The film shown in Fig. 2A was spin coated from a chlorobenzene solution with 8.24 mg PCBM and 6.97 mg CyC ml<sup>-1</sup> solvent. The final morphology is composed of layered PCBM domains extending above the CyC layer covering the substrate (Fig. 2C). This suggests that the film formation proceeds via a transient bilayer followed by rupture. PCBM forms the top layer and decomposes into droplets that penetrate CyC. Thereby, CyC is pushed aside and accumulates in a rim surrounding the PCBM. These topographical features are clearly visible in Fig. 2B. For this film, the Fourier transform of the surface showed a peak at 365 nm for the top PCBM layer, and two peaks at 410 nm and 156 nm for CyC after PCBM removal. The appearance of dominant length scales suggests a spinodal mechanism is driving the phase separation process.

A second example of phase separated morphologies is shown in Fig. 2E-H. Both films ruptured in this case and lateral fully separated PCBM domains within the CyC layer were formed. These domains extend from the substrate until above the cyanine matrix surface level (Fig. 2G). Wavelengths that characterize this film are 1380 nm for PCBM, and 498 nm such as 2490 nm for CyC.

The phase separation process follows some general trends. A common structural feature for films with thickness ratios of PCBM to CyC below  $\sim 1$  was that PCBM decomposed into isolated domains while CyC was the continuous, film forming matrix. With increasing PCBM content a stability transition occurred and CyC became the structure forming component. Finally, the morphology transformed into a bilayer system with dewetting holes, with PCBM against the air interface and CyC against the substrate. We found that similar morphologies develop for films with similar thickness ratios of PCBM to CyC, and that the individual film thicknesses are less important for the overall structure that develops. These values have an influence on the length scales of the lateral dimensions, and for a given morphology type the dimensions decrease with decreasing film thicknesses.

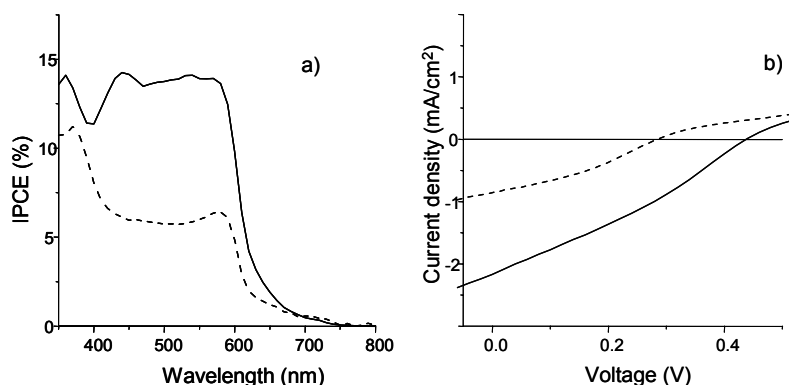


Fig. 3. Incident photon-to-electron conversion (IPCE) efficiencies (a), and current-voltage data (b) of ITO/PEDOT(80 nm)/CyC:PCBM/C<sub>60</sub>(30 nm)/Al(40 nm) solar cells. Films as shown in Fig. 2 were used as the active PCBM/CyC layer for device fabrication (full lines in Fig. 3 are results using the film of Fig. 2A, dashed lines correspond to the film of Fig. 2E). White-light ( $P_{in} = 100 \text{ mW cm}^{-2}$ ) I-V characteristics were  $V_{oc} = 0.44 \text{ V}$ ,  $I_{sc} = -2.18 \text{ mA cm}^{-2}$ ,  $FF = 30 \%$ ,  $\eta = 0.29 \%$  for the full line, and  $V_{oc} = 0.29 \text{ V}$ ,  $I_{sc} = -0.86 \text{ mA cm}^{-2}$ ,  $FF = 34 \%$ ,  $\eta = 0.08 \%$  for the dashed line.  $V_{oc}$  and  $I_{sc}$  denote the open-circuit voltage and short-circuit current, respectively,  $FF = V_m \cdot I_m \cdot V_{oc}^{-1} \cdot I_{sc}^{-1}$  is the fill factor,  $V_m$  and  $I_m$  are the current density and voltage at maximum power output, and  $\eta = FF \cdot I_{sc} \cdot V_{oc} \cdot P_{in}^{-1}$  is the power conversion efficiency.

In Fig. 3 we show performance data of PCBM/CyC solar cells with the actual film morphologies of Fig. 2. To improve the diode behavior and to avoid direct contact between CyC and aluminium, a thin layer of C<sub>60</sub> was evaporated (see Discussion). Apparently, the morphology has a pronounced influence on performance. For wavelengths above approx. 500 nm, the IPCE is dominated by the cyanine contribution, however, current is also generated at smaller wavelengths, where PCBM absorbs. This indicates that both the reductive electron transfer after photoexcitation of the donor CyC, as well the oxidative electron transfer after excitation of PCBM, are energetically allowed. The vertically stratified arrangement of Fig. 2C (full lines in Fig. 3) performs better than the laterally patterned film (Fig. 2G, dashed lines in

Fig. 3). Both the IPCE and the white light efficiency are improved by a factor of  $\sim 3$ , and for the I-V characteristic it is the higher short-circuit current and open-circuit voltage that cause the increase, while the fill factor is essentially the same for both configurations.

## DISCUSSION

Our experimental results suggest a transient bilayer film formation during spin coating, with PCBM at the air interface and CyC covering the substrate. A layered configuration is stable and PCBM wets finally the cyanine if the condition for the spreading coefficient  $S = \gamma_{\text{CyC}} - \gamma_{\text{PCBM}} - \gamma_{\text{PCy}} > 0$  is fulfilled<sup>16</sup>.  $\gamma_{\text{PCy}} = \gamma_{\text{PCBM}} + \gamma_{\text{CyC}} - 2(\gamma_{\text{PCBM}}\gamma_{\text{CyC}})^{1/2}$  denotes the surface tension between PCBM and CyC, respectively<sup>16</sup>, and  $\gamma_{\text{PCBM}}$  and  $\gamma_{\text{CyC}}$  are the surface tensions of the individual components. Interestingly, with the experimental values  $\gamma_{\text{PCBM}} = 23.9 \text{ mN m}^{-1}$ ,  $\gamma_{\text{CyC}} = 34.3 \text{ mN m}^{-1}$ , it follows that  $S = +9.5 \text{ mN m}^{-1}$ , and the bilayer configuration should be stable. This contradicts with the experimental observations, which means that additional forces are present during spin coating that amplify film thickness fluctuations and lead to rupture.

One potential source of instability may arise from the rapid solvent evaporation during spin coating that leads to concentration gradients in the solution and to evaporative cooling of the film surface. Such effects may drive convective flows that destabilize the film<sup>17</sup>. These Marangoni-like instabilities are expected to be important for low boiling solvents, whereas for high boiling solvents with a low evaporation rate, solvent diffusion through the film will be able to maintain a spatially uniform solvent concentration, so that the driving force for instability is removed<sup>18</sup>. The morphology features shown in Fig. 2 were obtained with chlorobenzene as the solvent, but using chloroform did not change their appearance. Also no change was observed when the solution was deposited on a heated ( $\sim 85^\circ\text{C}$ ) spin coater chuck to accelerate the evaporation rate even further. From these observations we tentatively exclude Marangoni-like convection flows from driving the bilayer instability.

We next discuss van der Waals forces. These omnipresent interactions arise from polarization fluctuations in the materials and are well known to affect the stability of thin films<sup>16,19-22</sup>. For two parallel layers, separated by a distance  $d$ , the interaction due to the dispersion forces is given by  $W = -A/(12\pi d^2)$ , with  $A$  the effective Hamaker constant for the film sandwiched between a substrate and gas (usually air). For this simple situation, the sign of  $A$  only determines the film stability. If  $A < 0$ , the system can gain energy by enlarging the distance  $d$  between the surfaces, and the film is stable. On the other hand, if  $A > 0$ , the film is unstable and breaks up; in that case, one expects to observe a dominant rupture wavelength arising from spinodal dewetting<sup>16,23</sup>.

In bilayer systems, additional terms have to be added to the simple equation for the single layer to approximately account for the multiple van der Waals contributions. The stability then no longer is predictable from the Hamaker constants only, but depends on the thickness of the individual layers<sup>19,22</sup>. However, the situation remains simple if all constants have the same sign. If all constants are negative, the bilayer is stable, and if they are all positive the system is unstable and both layers will spontaneously dewet. Referring to our bilayer system substrate(s, glass)/cyanine(1)/PCBM(2)/air(g), we obtained for the relevant three- and four-indices Hamaker constants  $A_{\text{g21s}} = -2.18 \cdot 10^{-20} \text{ J}$ ,  $A_{\text{21s}} = -0.43 \cdot 10^{-20} \text{ J}$  and  $A_{\text{12g}} = -0.97 \cdot 10^{-20} \text{ J}$  (see Experimental). Apparently, all constants have the same negative sign. It is known that the exact value of Hamaker constants depend on the method of calculation<sup>16</sup>, however, even a large variation of the experimentally determined value did not change the overall situation.

A second argument that conflicts with van der Waals forces being responsible for film break up arises when estimating the actual rupture time,  $\tau = 48\pi^2\eta d^5/A^2$ , with  $\eta$  the viscosity<sup>24</sup>.  $\tau$  corresponds to the characteristic growth time by which the unstable mode leading to spinodal dewetting is amplified. If  $\tau$  is long, this can indicate that dewetting by nucleation from defects is quicker and a spinodal wave has no chance to build up. In addition, for fabricating a thin film from solution,  $\tau$  must be shorter than the time during which the solvent evaporates and the film thins; after that, the system is frozen in.

A precise value for  $\tau$  can not be given for our experimental setup. Initially, a thick ( $> 1 \text{ mm}$ ) film is deposited on the substrate. During spin coating, excess material is removed in a first step, and afterwards the film thins as the solvent evaporates and vitrifies at the final thickness. During this time (a few seconds), all parameters that enter the calculation for  $\tau$  change continuously, and, for example, the viscosity will increase with solvent evaporation, while the thickness is decreasing. We also do not know at what thickness spinodal dewetting starts. We can reliably calculate the shortest rupture times inherently possible in the system, and, as an example, consider a hypothetical PCBM film that breaks up

very late during solvent evaporation (i.e.  $\gamma \sim 23.9 \text{ mN m}^{-1}$  from PCBM, and  $d \sim$  final thickness as measured), but that still has the viscosity of the starting solution (i.e.  $\eta \sim 0.799 \text{ mNs m}^{-2}$  from pure chlorobenzene). For this situation, we calculate rupture times  $\tau \sim 30 \text{ sec}$  and  $\sim 960 \text{ sec}$  for layer thicknesses  $d = 50$  or  $100 \text{ nm}$ , respectively. Apparently, these times are much longer than the relevant spin coating period, although films of comparable thicknesses break up by a spinodal mechanism (Fig. 2). This again indicates that van der Waals forces are not responsible for the spinodal film destabilization mechanism.

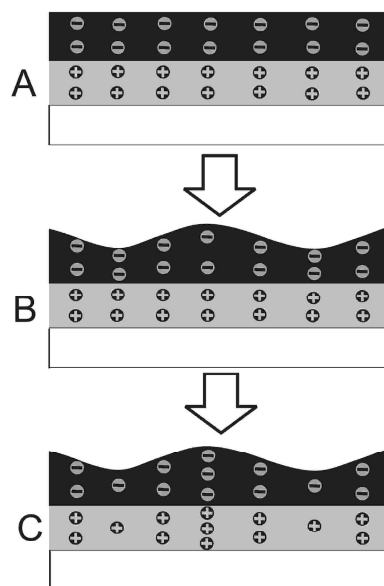


Fig. 4. Envisioned destabilization by electrostatic forces. It is entropically unfavorable to isolate the mobile counter ions in one of the phases and they will disperse partially in both of the phases. Effectively, the PCBM layer will be negatively charged, and the CyC layer will be positively charged (A). In the case of immobile or slow moving counter ions, any surface modulation would lead to an increased charge density in the thinner regions and a decreased charge density in the thicker regions (B). For mobile counter ions, though, the system will adapt a more uniform charge distribution. Charge adjustment will occur by recombination of charges in the thinner regions and dissociation in the thicker regions across the PCBM/CyC interface (C). Counter ion transfer is connected to a gain in free energy, which means the system can lower its free energy by dissociating more ion pairs than there will be recombining. Enhanced charge transfer is thus favored and the film destabilizes.

From this analysis, we conclude that van der Waals forces are probably not responsible for the experimental fact that PCBM/CyC thin films were always unstable. We also believe that convective flows during spin coating do not play a major role for the structure formation. A characteristic of our material system is that the cyanine dye is positively charged and associated by the negative  $\text{ClO}_4^-$  counter ion. This can give rise to electrostatic forces in thin films, and space charge can build up for example if  $\text{ClO}_4^-$  ions diffuse from the cyanine layer into the PCBM phase. As a result, the CyC layer will be positively charged, and the PCBM layer will be negatively charged.

The free energy of a bilayer due to this net charge is composed of an electrostatic contribution and an energy associated with the migration of mobile counter ions. Specific interactions between the counter ion and PCBM in combination with a gain in entropy can lead to spontaneous transfer of ions. Thereby, the system gains energy. Surface and interface fluctuations favour continuing ion transfer, which amplifies the film undulations and effectively destabilizes the film. The situation is depicted in Fig. 4. A detailed analysis of the dewetting scenario will be presented elsewhere; however, the mechanism implies that a fraction of perchlorate anions that diffuse across the junction get trapped in the PCBM phase at the moment the system vitrifies. We used XPS to proof that  $\text{ClO}_4^-$  anions indeed were present in PCBM. Mixed

PCBM/CyC films after selective dissolution of the dye were studied and  $\text{ClO}_4^-$  could clearly be detected. That the anions present are accompanied by the dye chromophore could be excluded: a UV-VIS spectrum of the dissolved PCBM phase did not reveal any CyC signature, while a comparison solution with the same  $\text{ClO}_4^-$  fraction, but now accompanied by the dye showed a clear CyC peak. This result suggests that CyC molecules were not trapped in the fullerene matrix and therefore readily dissolved.

It is interesting to compare blend film morphology with solar cell efficiency. Several structural features are beneficial for a high performance. For example, each material of the heterojunction should only be in contact with one of the electrodes<sup>3</sup>. Such vertically segregated structures optimize charge transport and reduce leakage current<sup>25-27</sup>. Pure phases of the two materials with continuous paths between the electrodes act as a parallel shunt resistance, as is apparent in a lowered open-circuit voltage. As mentioned above, there exists a tradeoff between a fine scale of phase separation (to optimize exciton dissociation) and a bicontinuous network with percolating paths to allow for efficient charge transport. Results from a dynamical Monte Carlo model clearly identified this optimum balance, and the highest device efficiency was obtained at an intermediate interfacial area<sup>28</sup>.

Our results nicely confirm some of these expectations (compare Fig. 2 with Fig. 3). The thickness of the cyanine layer was the same for both configurations. This ensures that the same amount of incident light is absorbed and allows a better comparison. Solar cells from as-prepared PCBM/CyC layers were not rectifying and were shorted. This is indeed expected, since for both films connecting paths for CyC exist between the cathode and anode, while PCBM forms connecting channels only in the laterally separated film (Fig. 2G). We therefore evaporated a thin layer of  $\text{C}_{60}$  between the active film and aluminium that serves as a blocking layer for holes at the cathode. However, the symmetry for the PCBM phase in Fig. 2G was thereby not broken, still resulting in potential current loss and a reduced open-circuit voltage. Indeed, the efficiency and the relevant parameters for the device fabricated from the lateral separated film were considerable lower (Fig. 3).

Apparently, also for the vertically segregated structure, the device efficiency ( $\eta = 0.29\%$ , Fig. 3b) is fairly low. One reason might be that the PCBM droplets that form in the CyC matrix are isolated from each other and no connecting network for electron transfer is present. This can decrease the charge mobility and result in increased bimolecular recombination, i.e. the collected current lowers. In addition, it leads to a strongly field dependent I-V characteristic when going from  $V = 0$  ( $I_{sc}$ ) to  $V_{oc}$ , as manifested in a low device fill factor ( $FF = 30\%$ , Fig. 3b).

Another reason for the low efficiency might be a low charge generation rate inherent to the material system. This is because both components are good electron acceptors and the energy difference between their lowest unoccupied molecular orbitals (LUMO) is small<sup>29</sup>. This may lower the driving force for electron transfer<sup>30</sup> after photoexcitation of CyC and decrease the initial number of charges formed per photon absorbed.

The phase separated domains for both films are in the range of several hundred nanometers. This is much larger than the exciton diffusion lengths ( $\sim 10$  nm), and any comparison between experimental device efficiency and interfacial area is not meaningful at this point. We are currently working on the issue of maintaining a certain type of morphology during spin coating of blend films, but varying the size of phase separated domains in a systematic way down to below 100 nm. We finally note that the schematic diagrams of Fig. 2C and Fig. 2G have to be interpreted with some care. Although selective dissolution allowed obtaining a good idea of the established morphology, AFM mainly reflects the in-plane separation evident at the sample surface. A more detailed picture will be obtained by cross-sectional analysis of these thin films.

## CONCLUSION

AFM snapshots revealed different morphologies obtained by spin coating thin films from blends of PCBM and a cationic dye from solution. We demonstrated that films form a transient bilayer which finally is destabilized through effective interface interactions. We propose a model that describes a film destabilization mechanism of electrostatic origin. The structures finally observed are governed not only by the phase behaviour of the materials blend, but might depend on the non-equilibrium conditions the films were prepared. A simple explanation of the dewetting process captures the basic

features, but continuing studies on the driving mechanism of instability during spin coating are necessary to confirm the details of the models.

Photovoltaic devices were fabricated and performance figures were related to the internal film structure. Experimental results on morphology/efficiency relationships of heterojunction solar cells are rare, simply because it is generally very difficult to control the thin film formation process, such that phase separated domains over a wide range of interfacial area are formed. In our material system, the domain size depends mainly on the film thickness which can be varied easily. Thus, much smaller domains than the features observed here can be produced. This will allow deriving more quantitative aspects of the dependence of the efficiency on the heterojunction film morphology. An understanding of these mechanisms is of crucial importance for the performance increase of such organic thin-film devices.

## Acknowledgements

We thank S. Huber for the synthesis of the dye CyC, T. Kuenniger for the dynamic contact angle measurements and U. Müller for the XPS measurements. We acknowledge funding from COST action P12, and thank the Swiss Scanning Probe Microscopy User Laboratory at Empa for support with the AFM measurements.

## REFERENCES

- [1] Lloyd, M. T., Anthony, J. E. and Malliaras, G. G., "Photovoltaics from soluble small molecules", *Mater. Today* 10(11), 34-41 (2007).
- [2] Mayer, A. C., Scully, S. R., Hardin, B. E., Rowell, M. W. and McGehee, M. D., "Polymer-based solar cells", *Mater. Today* 10(11), 28-33 (2007).
- [3] Günes, S., Neugebauer, H. and Sariciftci, N. S., "Conjugated polymer-based organic solar cells", *Chem. Rev.* 107, 1324-1338 (2007).
- [4] Xue, J., Rand, B. P., Uchida, S. and Forrest, S. R., "A hybrid planar-mixed molecular heterojunction photovoltaic cell", *Adv. Mater.* 17, 66-71 (2005).
- [5] Castro, F. A., Benmansour, H., Graeff, C. F. O., Nüesch, F., Tutis, E. and Hany, R., "Nanostructured organic layers via polymer demixing for interface-enhanced photovoltaic cells", *Chem. Mater.* 18, 5504-5509 (2006).
- [6] Castro, F. A., Graeff, C. F. O., Heier, J. and Hany, R., "Interface morphology of vertically segregated thin films of semiconducting polymer/polystyrene blends", *Polymer* 48, 2380-2386 (2007).
- [7] Geoghegan, M. and Krausch, G., "Wetting at polymer surfaces and interfaces", *Prog. Polym. Sci.* 28, 261-302 (2003).
- [8] Reiter, G., "Dewetting of thin polymer films", *Phys. Rev. Lett.* 68, 75-78 (1992).
- [9] Bandyopadhyay, D. and Sharma, A., "Nonlinear instabilities and pathways of rupture in thin liquid bilayers", *J. Chem. Phys.* 125, 054711 (2006).
- [10] Müller-Buschbaum, P., Bauer, E., Wunnicke, O. and Stamm, M., "The control of thin film morphology by the interplay of dewetting, phase separation and microphase separation", *J. Phys.: Condens. Matter* 17, S363-S386 (2005).
- [11] Geiger, T., Benmansour, H., Fan, B., Hany, R. and Nüesch, F., "Low-band gap polymeric cyanine dyes absorbing in the nir region", *Macromol. Rapid Comm.* 2008, accepted for publication.
- [12] Ma, W., Yang, C., Gong, X., Lee, K. and Heeger, A. J., "Thermally stable, efficient polymer solar cells with nanoscale control of the interpenetrating network morphology", *Adv. Funct. Mater.* 15, 1617-1622 (2005).



- [13] Horcas, I., Fernández, R., Gómez-Rodríguez, J. M., Colchero, J., Gómez-Herrero, J. and Baro, A. M., "A software for scanning probe microscopy and a tool for nanotechnology", *Rev. Sci. Instrum.* 78, 013705 (2007).
- [14] Owens, D. K. and Wendt, R. C., "Estimation of the surface free energy of polymers", *J. Appl. Polym. Sci.* 13, 1741-1747 (1969).
- [15] Kaelble, D. H., "Dispersion-polar surface tension properties of organic solids", *J. Adhes.* 2, 66-81 (1970).
- [16] Israelachvili, J. N., In "Intermolecular and surface forces", 2<sup>nd</sup> ed.; Academic Press: London (1992).
- [17] Luo, S.-C., Craciun, V. and Douglas, E. P., "Instabilities during the formation of electroactive polymer thin films", *Langmuir* 21, 2881-2886 (2005).
- [18] Heriot, S. Y. and Jones, R. A. L., "An interfacial instability in a transient wetting layer leads to lateral phase separation in thin spin-cast polymer-blend films", *Nature Mater.* 4, 782-786 (2005).
- [19] de Silva, J. P., Geoghegan, M., Higgins, A. M., Krausch, G., David, M.-O. and Reiter, G., "Switching layer stability in a polymer bilayer by thickness variation", *Phys. Rev. Lett.* 98, 267802 (2007).
- [20] Seemann, R., Herminghaus, S. and Jacobs, K., "Gaining control of pattern formation of dewetting liquid films", *J. Phys.: Condens. Matter* 13, 4925-4938 (2001).
- [21] Seemann, R., Herminghaus, S., Neto, C., Schlagowski, S., Podzimek, D., Konrad, R., Mantz, H. and Jacobs, K., "Dynamics and structure formation in thin polymer melt films", *J. Phys.: Condens. Matter* 17, S267-S290 (2005).
- [22] Govor, L. V., Parisi, J., Bauer, G. H. and Reiter, G., "Instability and droplet formation in evaporating thin films of a binary solution", *Phys. Rev. E* 71, 051603 (2005).
- [23] Steiner, U., "Structure formation in polymer films", In "Nanoscale assembly – chemical techniques", ed. W. T. S. Huck, New York: Springer (2005).
- [24] Pototsky, A., Bestehorn, M., Merkt, D. and Thiele, U., "Alternative pathways of dewetting for a thin liquid two-layer film", *Phys. Rev. E* 70, 025201(2004).
- [25] Arias, A. C., Corcoran, N., Banach, M., Friend, R. H., MacKenzie, J. D. and Huck, W. T. S., "Vertically segregated polymer-blend photovoltaic thin-film structures through surface-mediated solution processing", *Appl. Phys. Lett.* 80, 1695-1697 (2002).
- [26] Arias, A. C., "Vertically segregated polymer blends: their use in organic electronics", *J. Macromol. Sci. C (Polymer Reviews)* 46, 103-125 (2006).
- [27] Geiser, A., Fan, B., Benmansour, H., Castro, F., Heier, J., Keller, B., Mayerhofer, K. E., Nüesch, F. and Hany, R., "Poly(hexylthiophene)/C<sub>60</sub> heterojunction solar cells: implication of morphology on performance and ambipolar charge collection", *Solar Energy Mater. & Solar Cells* 92, 464-473 (2008).
- [28] Watkins, P. K., Walker, A. B. and Verschoor, G. L. B., "Dynamical monte carlo modelling of organic solar cells: the dependence of internal quantum efficiency on morphology", *Nano Lett.* 5, 1814-1818 (2005).
- [29] Fan, B., Hany, R., Moser, J.-E. and Nüesch, F., "Enhanced cyanine solar cell performance upon oxygen doping", *Org. Electronics* 9, 85-94 (2008).
- [30] Rand, B. P., Burk, D. P. and Forrest, S. R., "Offset energies at organic semiconductor heterojunctions and their influence on the open-circuit voltage of thin-film solar cells", *Phys. Rev. B* 75, 115327 (2007).